Uncovering air-sea interaction in oceanic submesoscale frontal regions using high-resolution satellite observations

Alex Ayet[1,2,3], Nicolas Rascle[4], Bertrand Chapron[5], Fleur Couvreux[2], and Laurent Terray[3]

[1]Université Grenoble Alpes, CNRS, Inria, Grenoble INP, GIPSA-Lab, France
[2]Université de Toulouse, Météo-France, CNRS, CNRM, France
[3]Université de Toulouse, CNRS, CERFACS, CECI, France
[4]Centro de Investigación Científica y de Educación Superior de Ensenada (CICESE), México
[5]Ifremer, CNRS, IRD, Université de Bretagne Occidentale, IUEM, LOPS, France

In an enthusiastic paper 20 years ago, R. A. Brown suggested that remote sensing measurements of the ocean surface reaching resolutions of ten to hundreds of meters over 1000-km regions would open a new realm for analysis, modelling, and understanding of the atmospheric and oceanic boundary layers (Brown 2000). Twenty years later, it is too early to state that all physical processes have been extracted from those measurements. However, today, theoretical planetary boundary-layer work combined with high-resolution numerical simulations can pave the way for analysis strategies that can be systematically applied to ocean remote sensing observations. There is now hope for the serendipitous features appearing in remote sensing data to be systematically exploited. In this article we discuss what we expect to learn regarding air-sea interactions at small scales.

Active microwave synthetic aperture radars (SARs) and optical radiometers (viewing areas in and around the sunglint) are sensitive to instantaneous ocean surface roughness contrasts. Those contrasts result from variations of the steepness of short gravity and capillary waves due to their interactions with (i) an inhomogeneous near-surface wind field, (ii) nonuniform surface currents, and (iii) surface slicks accumulated by surface current convergences which suppress short waves (Alpers 1985; Munk et al. 2000; Kudryavtsev et al. 2005, 2012). The typical relaxation time and space scales of these short surface waves are smaller than 1 s and 100 m, which implies that the roughness contrast images offer a quasi-instantaneous picture of the air-sea interface.

These variations of the air-sea interface roughness are controlled by the dynamical and thermodynamical processes occurring in the marine atmospheric boundary layer (MABL, of height O(500 m)) and in the ocean mixed layer (OML, of depth O(50 m)), both of which are coupled over a wide range of spatio-temporal scales. In ocean frontal regions this coupling is particularly intense.

Ocean fronts can affect the MABL, inducing strong near-surface wind heterogeneities, which could then impact the OML. There is thus hope that the *imprint* of the MABL-OML coupling can be quantified through remotely sensed roughness contrasts, helping to advance the understanding of ocean-atmosphere interactions. More precisely, these high-resolution images could help better understand the transfers of heat and momentum between the ocean and atmosphere, which depend on the mixing processes (both vertical and horizontal) in the MABL and the OML, and which are essential for weather and climate models. Many spectacular manifestations of MABL and OML processes are now routinely reported in roughness images. One typical example is convection organization in the MABL, illustrated in the top panel of Figure 1, which can transition from two-dimensional rolls (with scales of 1-10 km) to three-dimensional convective cells (Atkinson and Zhang 1996). This is illustrated in Figure 2a, where Boxes 1 and 3 show typical signatures of these two- and three-dimensional MABL coherent structures respectively (as defined in Wang et al. 2020). This measurable organization can then be used to

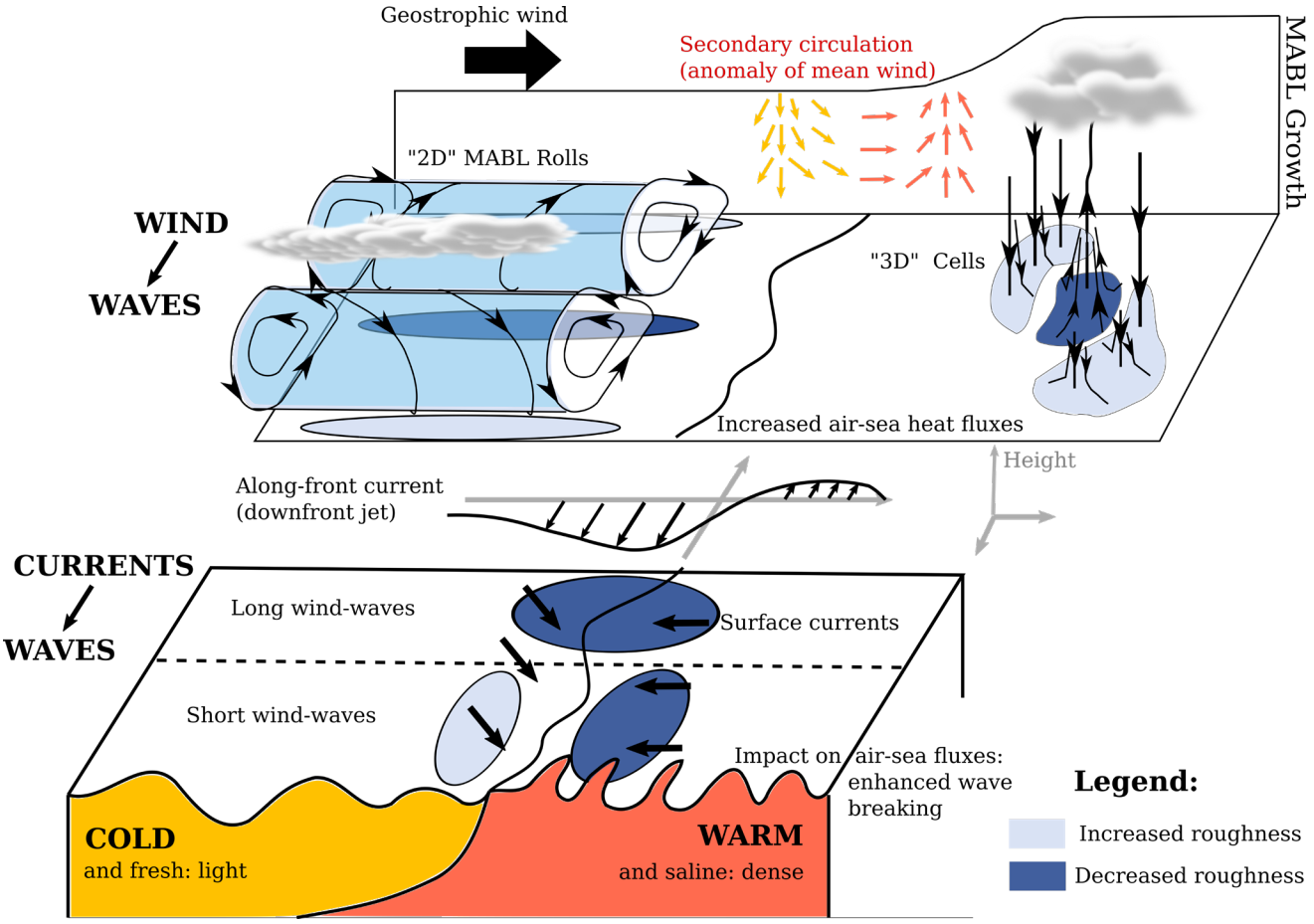

Figure 1. Sketch of the atmospheric (top panel) and oceanic (bottom panel) processes around an oceanic current front discussed in this paper. Top panel: The changes in air-sea heat fluxes and advective effects influence the MABL height and the convection organization, which can transition from MABL rolls to convective cells, thus impacting clouds and radiation. The mean wind is also affected, and secondary circulations can appear. Bottom panel: Surface currents interact with wind-waves, affecting their slope and distribution. The resulting effect depends on the wavelength of the waves. Those processes are believed to produce signatures on the sea-surface roughness, which is measurable through SARs or optical radiometers. The increased and decreased roughness areas correspond respectively to white and dark areas in Figures 2 and 4. The sketch is not to scale.

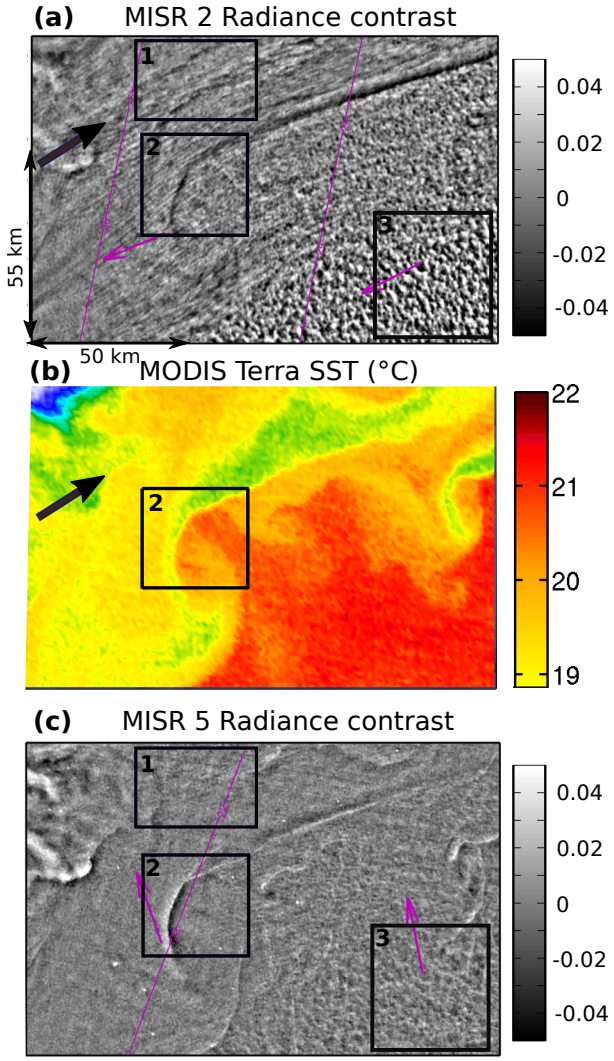

Figure 2. Quasi-simultaneous images of surface roughness and SST in the Northern Gulf of Mexico on February 11, 2016. (a) Sunglint images from Multiangle Imaging SpectroRadiometer (MISR, Chust and Sagarminaga 2007) camera #2, (b) SST from MODIS Terra, (c) Same as (a) but for MISR camera #5 viewing at a different angle. Magenta contours and arrows in (a) and (c) show respectively zenith and azimuth view angles (defined as the angles to reflect sunlight towards the satellite).

determine changes in local wind stress direction and magnitude (Beal et al. 1997; Weckwerth et al. 1997). By relying on the similarity relationships of the convective MABL, the images can also be used to infer other MABL properties such as its height (Sikora et al. 1997) and some of its turbulence statistics (Young et al. 2000). Surface roughness images also show manifestations of fine-scale current fronts at the ocean sub-mesoscale (spatial scales below 10 km). This is illustrated in the bottom panel of Figure 1 and in Figure 2a, where Box 2 shows an oceanic front, which despite being elongated over more than 10 km, is only about 50 m wide. Current gradients at this front are confirmed by in-situ buoy measurements to reach 100 f (f being the Coriolis frequency), thus largely escaping the geostrophic equilibrium (D'Asaro et al. 2018; Rascle et al 2020). Due to the large vertical velocities they induce, those fronts are hot spots for biology and drifting pollution, including plastics and seaweeds. Furthermore, current fronts are also associated with intense sea surface temperature (SST) fronts, as illustrated in the bottom panel of Figure 1, which can affect the MABL by impacting air-sea heat fluxes. The dynamics occurring at these strong frontal zones are still poorly understood, involving most probably active feedbacks between MABL, OML, and surface waves. The following section illustrates how remote sensing roughness observations could help advance our physical knowledge of those processes.

Wave-current interactions and their signature on roughness images

Around intense current fronts, at typical scales of 0.1-1 km, wave-current interactions are the dominant source of sea surface roughness contrast. For this range of scales, surface roughness directly traces the effect of current on surface waves. This effect can be inverted to estimate current fields from surface roughness observations.

Despite its apparent simplicity, this inversion involves two fairly different dynamical regimes. Very short wind-waves are in tight equilibrium with the local wind and respond quasi-locally and instantaneously when perturbed by a current gradient. On the contrary, longer wind-waves have significant propagation and response length scales before reaching back their equilibrium with the local wind (e.g., Phillips 1984). Note that here we discuss short and long wind-waves, whereas freely propagating swell

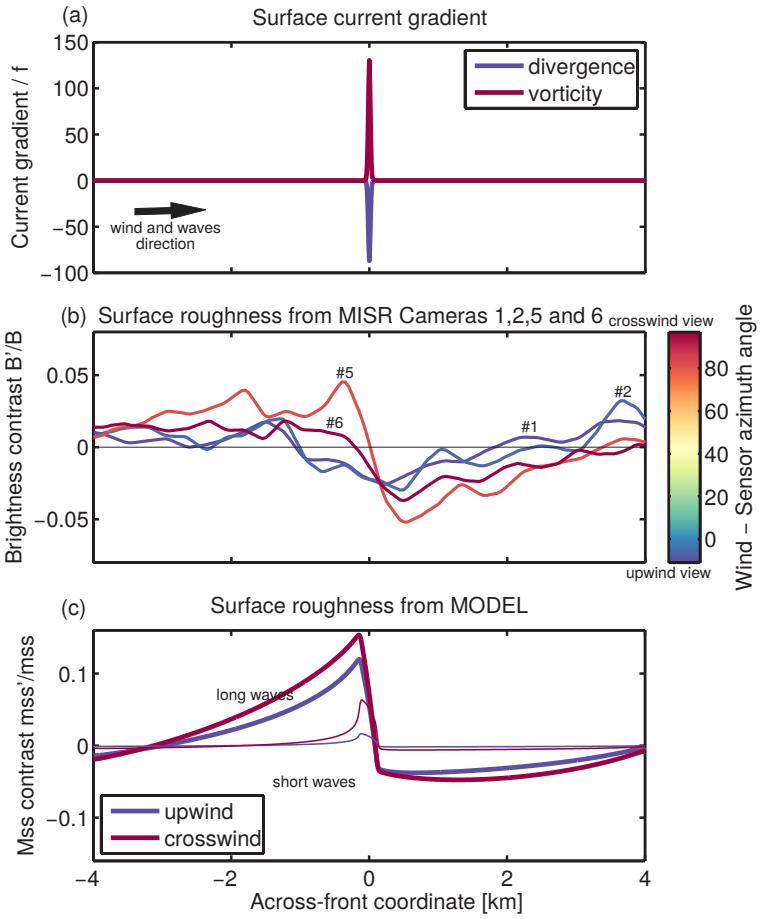

Figure 3. Transect of the current front of zone 2 of Figure 2. A sketch of the frontal currents can be found in the bottom panel of Figure 1. (a) Current gradient estimates from buoy observations at the front. (b) Surface roughness contrasts (defined here as brightness contrast) from selected MISR cameras. (c) Surface roughness contrasts (defined here as mean square slope (mss)) calculated from the wave-current interaction model of Kudryavtsev et al. (2005). Mss is divided here into upwind and crosswind components, and into long waves (k<0.6 rad/m) and short waves (k>30 rad/m) contributions.

follows yet another distinct dynamical regime (e.g. Villas Bôas et al. 2020). In addition to wavelength, wave direction relative to the current gradient is also important for refraction and/or wave steepening. Each component of the directional wave spectrum thus responds differently to the current perturbation. This is illustrated in Figure 2a and c. The two satellite roughness images were acquired quasi-simultaneously (4 minutes apart) but at different view angles (shown in magenta), which is equivalent to selecting different components of the directional wave field. It is apparent that the current front in zone 1 has two different signatures on the roughness images: a negative roughness anomaly in Figure 2a (and blue lines in Figure 3b), or a dipolar roughness anomaly in Figure 2c (and red lines in Figure 3b). Numerical simulations, using a wave model forced by the observed underlying current (Figure 3a) show, as expected, that the sharp current front induces a localized response of short waves, and a more gradual, dipolar response of long waves (Figure 3c) with a sensitivity depending on the relative direction of the waves.

These different frontal responses of the directional wave components can be exploited to retrieve information on the current field around the front. Indeed, if the frontal responses of all components were observed, then the complete current field could be retrieved. In practice, only a few components of the wave spectrum can be observed. From airborne sensors, observations of surface roughness at different view angles allow measuring enough directional components to retrieve the width, velocity shear and convergence of the current at the front (Rascle et al. 2017). From spaceborne sensors, only a few directional components can be observed (e.g. Figures 2a and c), except for the long waves that can be resolved by some sensors (e.g. Kudryavtsev et al. 2017; Ardhuin et al. 2021). The challenge is thus to develop an observing strategy to extract the current information from available surface roughness observations.

Sampling turbulence and boundary layer dynamics

Ocean frontal regions are also zones of intense interaction between SST fronts and the MABL. At the ocean mesoscale (10-100 km), these interactions have been studied through observations (Vandemark et al. 1997; Chelton et al. 2004), and they can affect both the ocean kinetic energy budget (e.g., Renault et al. 2016) and troposphere dynamics (e.g., Foussard et al. 2019).

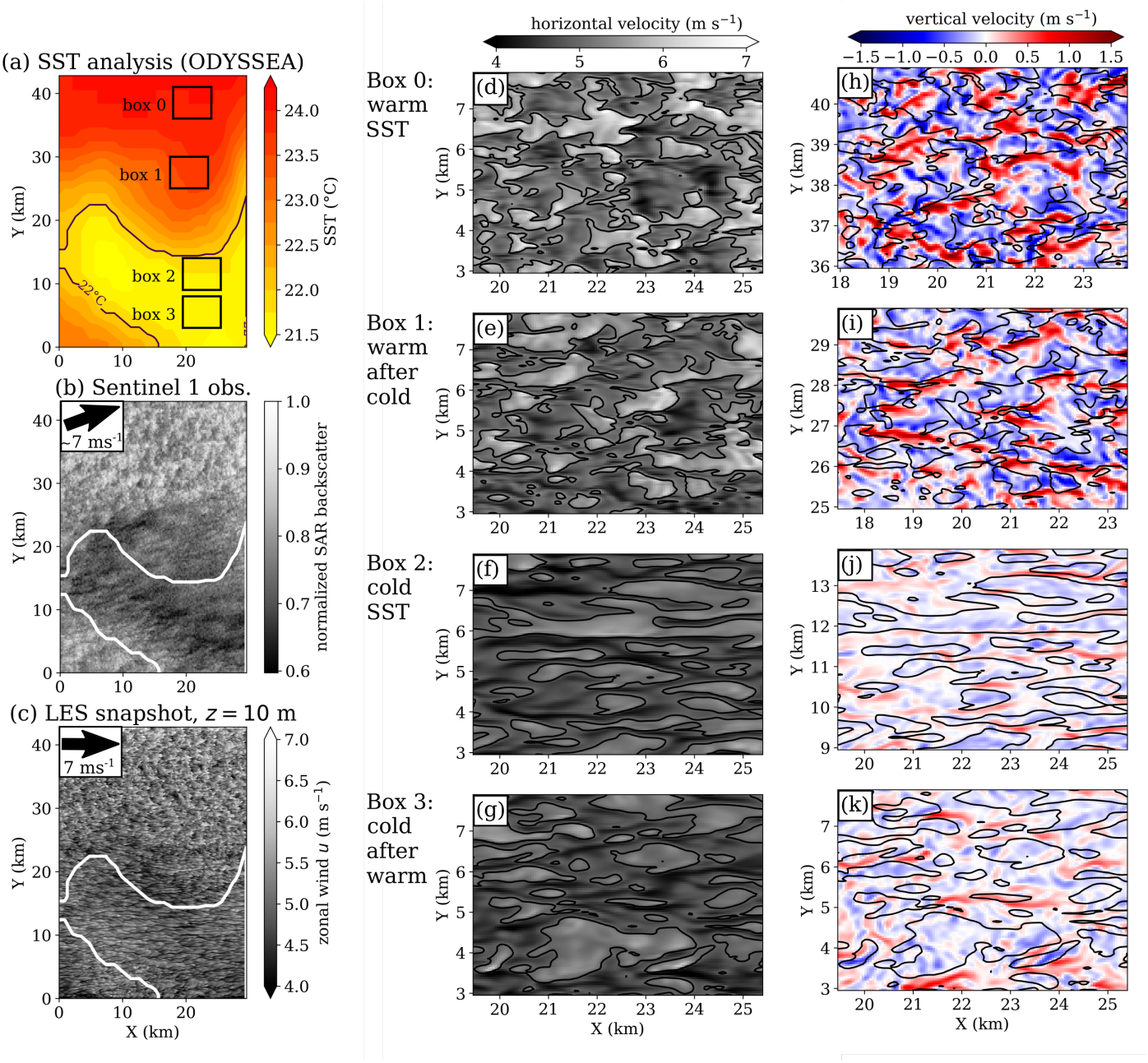

Figure 4. (a) SST analysis used to force the Large Eddy Simulation (LES) and (b) co-located surface roughness observation from Sentinel 1 (filtered at a 200m resolution). (c) Instantaneous 10-m zonal wind from the LES after reaching a quasi-equilibrium state. In (b) and (c) the black arrow indicates the observed wind direction/speed [in (b)], and the geostrophic direction/speed used to force the LES [in (c)]. Instantaneous quantities from the atmospheric LES in each of the boxes of Figure 4 (a). [(d)-(g)] Instantaneous zonal wind speed at 10-m height. Here and in [(h)-(k)], black contours indicate regions where the 10-m zonal wind exceeds its horizontal average over the box by 5%. [(h)-(k)] Instantaneous vertical wind speed at the middle of the boundary layer. Note that, in the LES, moisture, clouds, precipitation, and radiative fluxes are not considered.

However, little is known at the small scales discussed in the previous section (below 10 km), where nonlinear MABL dynamics are expected to become dominant (e.g., Sullivan et al. 2020). A case study in the Agulhas current, for which a submesoscale SST front was observed, illustrates how roughness images can help address this problem (Figure 4a, about 1°C over 10 km). The co-located roughness (SAR) image (Figure 4b) exhibits different textures, which are reminiscent of the convection-related signatures discussed in Figure 2a and the introduction.

The MABL physics behind these fine-scale structures is investigated using a high-resolution simulation (Large Eddy Simulation, LES, using the Meso-NH model, Lac et al. 2018) with horizontal resolution of 50 m and a vertical resolution varying from 2 m close to the surface to 20 m at 2 km height (the top of our domain). The simulation is forced by a homogeneous wind, and by the observed SST (Figure 4a) as a fixed-in-time bottom boundary condition, which impacts surface heat and momentum fluxes. Hence, all horizontal heterogeneities observed in the simulation can be attributed to the influence of the heterogeneous SST field on the MABL.

Figure 4c shows a snapshot of the simulated 10-m zonal wind speed over the simulation domain. It is strongly heterogeneous, with different textures comparable to those of Figure 4b, with however several differences: (i) the scale of the structures is larger in the SAR observation than in the LES; and (ii) the orientation of the structures is not the same in the LES (aligned in the zonal direction) than in the SAR image (where there is a meridional tilt). This second difference (ii) is an effect of the idealized LES set-up, for which a purely zonal wind has been imposed to ensure periodic boundary conditions (instead of the slightly tilted observed wind, shown in Figure 4b). As for difference (i), it could be attributed to a filtering effect of wind-waves. Due to their adjustment timescale, remotely-sensed wind-waves could end up being sensitive only to large enough atmospheric scales. Nonetheless, what the simulation shows is that the presence of different textures in the SAR observation can be attributed to the effect of the SST on the MABL.

A closer look to the different simulated textures in Figure 4d-g shows that, on the cold side of the domain (Figure 4f), the zonal wind structures are more elongated than on its warm side (Figure 4d and 4e). Those zones of strong zonal surface wind are well correlated with the downward vertical velocities at the middle of the MABL (compare black contours and red zones in Figures 4h-k). This shows that these near surface textures can be related to different organizations of convection and to coherent structures in the MABL (which transport high-momentum fluid downward, see the top panel of Figure 1): three-dimensional cells for a warmer SST (Boxes 0 and 1) and two-dimensional rolls for a colder SST (Box 2).

The case of Box 3 is however interesting. Even though the SST is similar to Box 2 in this area, the organization of convection does not have the same characteristic scales as Box 2. It is a transition regime between the three-dimensional cells of Boxes 0 and 1 and the rolls of Box 2. The MABL height of Box 3 (450 m) is also larger than the one in Box 2 (350 m, not shown). This shows that for these sharp frontal configurations, SST is not the only driver of MABL dynamics, and that advective effects could also play a role (see e.g., Sullivan et al. 2020). These changes are also associated with secondary circulations (see the sketch in the top panel of Figure 1), of particular interest to modelers as they relate to large-scale divergence (see e.g., the analytical formulas in Ayet and Redelsperger 2019) and affects the free troposphere (e.g., Feliks et al. 2004; Foussard et al. 2019).

Conclusion and outlook

This paper illustrates that high-resolution remote sensing images of ocean surface roughness, combined with theoretical and high-resolution numerical models, can provide physical insights into the air-sea interactions happening in intense ocean frontal regions. In particular: (i) local variations in surface roughness (due to currents and winds) can be detected; (ii) strong near-surface currents can be quantified; and (iii) changes in atmospheric convective organization and secondary circulations can be quantified and

attributed to SST-MABL interactions. For (ii) and (iii), the paper highlights the limitations of the methodologies used to extract information from the images, which require a deeper understanding of wind-wave-current interactions (see also Villas Bôas and Pizzo, this issue).

A lot still remains to be done in order to understand the coupled MABL-OBL system at fine scales. While some hints about the effect of SST gradients on the MABL exist, the effect of the strong current fronts on the MABL, through changes in surface roughness, is still not assessed. Those non-local changes affect whitecap coverage and should thus change ocean-atmosphere fluxes of momentum, heat, and gas. Wave-current coupling and ocean-atmosphere coupling thus become largely entangled. The changes in MABL convection organization also have important implications: (i) they likely affect the cloud organization and radiative properties of the MABL (Villefranque 2019); and (ii) they could affect the OML and its mixing properties. Point (i) highlights the need to use multimodal sensors that are capable of measuring cloud properties, roughness, currents, and SST almost simultaneously. Missions including multimodal sensors include the upcoming SWOT (Morrow et al. 2019), foreseen Harmony (ESA 2020) and proposed Seastar (Gommenginger et al. 2019) mission concepts. Point (ii) still remains to be assessed, and could require (a) understanding of how higher-order quantities of the current field, like secondary circulations and Langmuir circulations, can be extracted from roughness images and (b) using high-resolution coupled numerical simulations, which are still not at hand.

Nonetheless, a new age in the use of near-surface ocean observations and high-resolution numerical simulations is gradually emerging. Thinking about climate models, roughness images provide data-rich statistics about MABL-OML fine-scale coupling processes that can be used to constrain the development of new parameterizations and included in model evaluation metrics. We believe that properly using this information requires a combination of both observations, simulations and theory, which means developing dedicated, physic-informed statistical methods able to extract physical laws from multimodal remote sensing data.

Acknowledgments

AA thanks Fabrice Collard for providing the satellite data for the simulation as well as for the interesting discussions. AA was funded by a CNES post-doctoral grant. We acknowledge the use of The Atmospheric Science Data Center (ASDC) at NASA Langley Research Center for the MISR data.

References

Alpers, W., 1985: Theory of radar imaging of internal waves. *Nature*, **314**, 245-247, doi:10.1038/314245a0.

Ardhuin, F., M. Alday, and M. Yurovskaya, 2021: Total surface current vector and shear from a sequence of satellite images: Effect of waves in opposite directions. *J. Geophys. Res.: Oceans*, **126**, doi:10.1029/2021JC017342.

Atkinson, B. W., and J. Wu Zhang, 1996: Mesoscale shallow convection in the atmosphere. *Rev. Geophys.*, **34**, 403-431, doi:10.1029/96RG02623.

Ayet, A., and J.-L. Redelsperger, 2019: An analytical study of the atmospheric boundary-layer flow and divergence over an SST front. *Quart. J. Roy. Meteor. Soc.*, **145**, 2549-2567, doi:10.1002/qj.3578.

Beal, R. C., V. N. Kudryavtsev, D. R. Thompson, S. A. Grodsky, D. G. Tilley, V. A. Dulov, and H. C. Graber, 1997: The influence of the marine atmospheric boundary layer on ERS 1 synthetic aperture radar imagery of the Gulf Stream. *J. Geophys. Res.: Oceans*, **102**, 5799-5814, doi:10.1029/96JC03109.

Brown, R. A., 2000: Serendipity in the use of satellite scatterometer, SAR, and other sensor data. *Johns Hopkins APL Tech. Dig.*, **21**, 21-26.

Chelton, D. B., M. G. Schlax, M. H. Freilich, and R. F. Milliff, 2004: Satellite measurements reveal persistent small-scale features in ocean winds. *Science,* **303**, 978–983, doi:10.1126/science.1091901.

Chust, G., and Y. Sagarminaga, 2007: The multi-angle view of MISR detects oil slicks under sun glitter conditions. *Remote Sens. Environ.*, **107**, 232-239, doi:10.1016/j.rse.2006.09.024.

D'Asaro, E. A., and Coauthors, 2018: Correction for D'Asaro et al., Ocean convergence and the dispersion of flotsam. *Proc. Natl. Acad. Sci.*, **115**, doi:10.1073/pnas.1802701115.

ESA, 2020: Report for assessment: Earth Explorer 10 Candidate Mission Harmony. 133 pp, https://esamultimedia.esa.int/docs/EarthObservation/EE10_Harmony_Report-for-Assessment-v1.0_13Nov2020.pdf.

Feliks, Y., M. Ghil, and E. Simonnet, 2004: Low-frequency variability in the midlatitude atmosphere induced by an oceanic thermal front. *J. Atmos. Sci.*, **61**, 961-981, doi:10.1175/1520-0469(2004)061<0961:LVITMA>2.0.CO;2.

Foussard, A., G. Lapeyre, and R. Plougonven, 2019: Storm track response to oceanic eddies in idealized atmospheric simulations. *J. Climate*, **32**, 445-463, doi:10.1175/JCLI-D-18-0415.1.

Gommenginger, C., and Coauthors, 2019: SEASTAR: A mission to study ocean submesoscale dynamics and small-scale atmosphere-ocean processes in coastal, shelf and polar seas. *Front Mar. Sci.*, **6**, doi:10.3389/fmars.2019.00457.

Kudryavtsev, V., D. Akimov, J. Johannessen, and B. Chapron, 2005: On radar imaging of current features: 1. Model and comparison with observations. *J. Geophys. Res.: Oceans*, **110**, doi:10.1029/2004JC002505.

Kudryavtsev, V., A. Myasoedov, B. Chapron, J. A. Johannessen, and F. Collard, 2012: Imaging mesoscale upper ocean dynamics using synthetic aperture radar and optical data. *J. Geophys. Res.*, **117**, doi:10.1029/2011JC007492.

Kudryavtsev, V., M. Yurovskaya, B. Chapron, F. Collard, and C. Donlon, 2017: Sun glitter imagery of surface waves. Part 2: Waves transformation on ocean currents. *J. Geophys. Res.: Oceans*, **122**, 1384–1399, doi:10.1002/2016JC012426.

Lac, C., and Coauthors, 2018: Overview of the Meso-NH model version 5.4 and its applications. Geosci. Model Dev., 11, 1929-1969, doi:10.5194/gmd-11-1929-2018.

Morrow, R., and Coauthors, 2019: Global observations of fine-scale ocean surface topography with the Surface Water and Ocean Topography (SWOT) mission. *Front. Mar. Sci.*, **6**, doi:10.3389/fmars.2019.00232.

Munk, W., L. Armi, K. Fischer, and F. Zachariasen, 2000: Spirals on the sea. *Proc. Roy. Soc. London, Ser. A*, **456**, 1217-1280, doi:10.1098/rspa.2000.0560.

Phillips, O. M., 1984: On the response of short ocean wave components at a fixed wavenumber to ocean current variations. *J. Phys. Oceanogr.*, **14**, 1425-1433, doi:10.1175/1520-0485(1984)014<1425:OTROSO>2.0.CO;2.

Rascle, N., J. Molemaker, L. Marié, F. Nouguier, B. Chapron, B. Lund, and A. Mouche, 2017: Intense deformation field at oceanic front inferred from directional sea surface roughness observations. *Geophys. Res. Lett.*, **44**, 5599– 5608, doi:10.1002/2017GL073473.

Rascle, N., and Coauthors, 2020: Monitoring intense oceanic fronts using sea surface roughness: Satellite, airplane, and in situ comparison. *J. Geophys. Res.: Oceans*, **125**, doi:10.1029/2019JC015704.

Renault, L., M. J. Molemaker, J. C. McWilliams, A. F. Shchepetkin, F. Lemarié, D. Chelton, S. Illig, and A. Hall, 2016: Modulation of wind work by oceanic current interaction with the atmosphere. *J. Phys. Oceanogr.*, **46**, 1685-1704, doi:10.1175/JPO-D-15-0232.1.

Sikora, T. D., G. S. Young, H. N. Shirer, and R. D. Chapman, 1997: Estimating convective atmospheric boundary layer depth from microwave radar imagery of the sea surface. *J. Appl. Meteor.*, **36**, 833-845, doi:10.1175/1520-0450(1997)036<0833:ECABLD>2.0.CO;2.

Sullivan, P. P., J. C. McWilliams, J. C. Weil, E. G. Patton, and H. J. Fernando, 2020: Marine boundary layers above heterogeneous SST: Across-front winds. *J. Atmos. Sci.*, **77**, 4251-4275, doi:10.1175/JAS-D-20-0062.1.

Vandemark, D., J. B. Edson, and B. Chapron, 1997: Altimeter estimation of sea surface wind stress for light to moderate winds. *J. Atmos. Oceanic Technol.*, **14**, 716-722, doi:10.1175/1520-0426(1997)014<0716:AEOSSW>2.0.CO;2.

Villas Bôas, A. B., B. D. Cornuelle, M. R. Mazloff, S. T. Gille, and F. Ardhuin, 2020: Wave–current interactions at meso- and submesoscales: Insights from idealized numerical simulations. *J. Phys. Oceanogr.*, **50**, 3483-3500, doi:10.1175/JPO-D-20-0151.1.

Villefranque, N., 2019: Les effets radiatifs 3D des nuages de couche limite: De leur simulation explicite à leur paramétrisation. PhD dissertation, Université Paul Sabatier - Toulouse III, 274 pp, https://tel.archives-ouvertes.fr/tel-02628562/document.

Wang, C., D. Vandemark, A. Mouche, B. Chapron, H. Li, and R. C. Foster, 2020: An assessment of marine atmospheric boundary layer roll detection using Sentinel-1 SAR data. *Remote Sens. Environ.*, **250**, doi:10.1016/j.rse.2020.112031.

Weckwerth, T. M., J. W. Wilson, R. M. Wakimoto, and N. A. Crook, 1997: Horizontal convective rolls: Determining the environmental conditions supporting their existence and characteristics. *Mon. Wea. Rev.*, **125**, 505-526, doi:10.1175/1520-0493(1997)125<0505:HCRDTE>2.0.CO;2.

Young, G. S., T. D. Sikora, and N. S. Winstead, 2000: Inferring marine atmospheric boundary layer properties from spectral characteristics of satellite-borne SAR imagery. *Mon. Wea. Rev.*, **128**, 1506-1520, doi:10.1175/1520-0493(2000)128<1506:IMABLP>2.0.CO;2.